Magnetic ordering at the edges of graphitic fragments: Magnetic tail interactions between the edge-localized states

Hosik Lee,[1] Young-Woo Son,[1] Noejung Park,[2] Seungwu Han,[3] and Jaejun Yu[1],*

[1]*School of Physics and Center for Strongly Correlated Materials Research, Seoul National University, Seoul 151-747, Korea*
[2]*Department of Applied Physics, Dankook University, Seoul 140-714, Korea*
[3]*Department of Physics, Ewha Womans University, Seoul 120-750, Korea*

To understand the formation mechanism of magnetic moments at the edges of graphitic fragments, we carry out first-principles density-functional calculations for the electronic and magnetic structures of graphitic fragments with various spin and geometric configurations. We find that interedge and interlayer interactions between the localized moments can be explained in terms of interactions between the magnetic tails of the edge-localized states. In addition, the dihydrogenated edge states as well as Fe ad-atoms at the edge are studied in regard to the magnetic order and proximity effects.

I. INTRODUCTION

Magnetic signals observed in a doped fullerene system,[1] following previous work on weak ferromagnetic orderings observed in highly oriented pyrolytic graphite (HOPG),[2] have attracted research interest in understanding the origin of magnetism in organic materials, in particular, those based on a molecule with unpaired electrons.[1,3] Various magnetic properties, including spin-glass-like behavior,[4] paramagnetic states,[5] and ferromagnetic states,[2,6–8] have been reported on carbon systems. In particular, observations of the stable ferromagnetism in glassy carbon[8] and in polymerized fullerenes[6] suggest the possibility of the intrinsic magnetism arising from only C atoms without magnetic impurities. Nevertheless, there exists a cautious view that some reports on the carbon magnetism might be related to the presence of magnetic impurities. Recently, a report on the ferromagnetism in graphite after proton irradiation[9] added another piece of evidence for intrinsic magnetism arising from only C atoms without magnetic impurities.

In parallel with numerous experimental endeavors, there have been a series of theoretical studies on the magnetism in graphitic fragments and related carbon materials. In a graphene sheet, the existence of a localized state at the zigzag edge, associated with flat π bands at the Fermi level, was first predicted with a tight-binding model,[10] which was later confirmed by first-principles calculations.[11,12] However, we previously showed that the magnetic instability due to the flat π bands was found to disappear when the graphene sheets (or graphitic fragments) are stacked.[13] Instead, the presence of dangling bonds at the zigzag edge turned out to be crucial for the ferromagnetic ordering at the edge, which is robust against the layer-by-layer stacking. Other models on the origin of carbon magnetism have also been proposed, such as the geometry with a negative Gaussian curvature[14] or defects in the graphene sheets.[15]

So far, most of theoretical works have focused on the existence of the magnetic moment either at the edge or at the defect site, which serves as an isolated magnetic entity. For macroscopically observable magnetic phenomena, such mag-

netic moments should align collectively through the ferromagnetic interaction between them. In this work, we focus on the magnetic interactions between local moments, which may result in the long-range magnetic ordering. To understand the magnetic interactions between the edge-localized states in the graphitic fragments, we carried out first-principles calculations on the electronic and magnetic structures of the graphitic strips with various widths and stacking configurations. It is shown that while the dangling bonds at the edge contribute mainly to the formation of local moments, the edge-localized π-orbital state with a long tail extending into the inner sites of the graphitic strips plays a crucial role in determining the sign and magnitude of interedge and interlayer coupling of the magnetic edge states. We also consider alternative origins of magnetism in graphitic fragments. For instance, to investigate the so-called "bearded edge" state,[16] which is a localized edge state at the dihydrogenated zigzag edge, we employ both first-principles and tight-binding methods. It is found that the bearded edge state arises from the change of the boundary condition associated with an additional hydrogen termination. The magnetic proximity effect by Fe atoms is also studied, but is found to be negligible.

II. MODEL GEOMETRY AND CALCULATION METHODS

We performed first-principles calculations based on the density-functional theory (DFT) (Refs. 17 and 18) within the local spin-density approximation (LSDA) by using the PWSCF plane-wave code.[19] We employ ultrasoft pseudopotentials[20] for the ionic potentials. The local density functional parametrized by Perdew and Wang is used for the exchange-correlation potential of the electrons system.[21] The plane-wave basis set with the kinetic energy cutoff of 30 Ry is used throughout the calculations.

A schematic illustration of the model geometry used in the calculations is given in Fig. 1. The graphitic strip has a zigzag pattern at both edges of the strip, forming a one-dimensional lattice along the x direction. Twice the minimal unit cell is used throughout the self-consistent calculations to
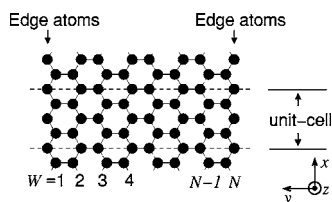
FIG. 1. A schematic drawing of the graphitic strip. The region between the two dashed lines indicates a unit cell for the antiferromagnetic spin configuration along the edge. (See details in the text.) The indices $W=1,2,\ldots,N$ correspond to each column of the zigzag chain.
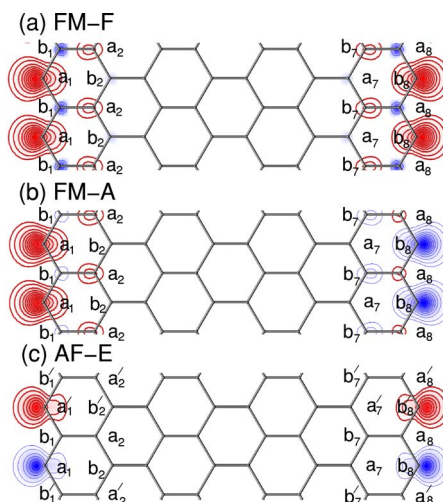

FIG. 2. (Color online) Contour plots of the electronic spin densities of an isolated strip with the open edge. (a), (b), and (c) correspond to the spin densities of FM-F, FM-A, and AF-E, respectively. Thicker lines indicate the up-spin density and thinner lines show the down-spin density. To display the sublattice magnetization feature clearly, the contour plots are made within the plane 0.6 Å above the strip layer containing the center of carbon atoms, where the positions of the carbon atoms in the primitive unit cell are shown at the bottom for clarity. Here the ball-and-stick drawing represents a unit cell.

allow for the antiferromagnetic ordering along the edge in x direction. (See Sec. III for the detailed description of magnetic structures.) As shown in Fig. 1, the width of the strip is defined by the number of columns, i.e., the number of zigzag chains along the x direction, and each zigzag column is labeled by the index running from 1 to N. Later, in Sec. IV, we investigate the interlayer interactions in the stacked graphitic strips.

In order to simulate isolated graphitic strips, we use a super-cell geometry where each plane is separated from its replica by 10 Å in both edge-to-edge and layer-to-layer directions. The atomic positions are adopted from the perfect graphite geometry. To check the relaxation effect, geometries of some systems are optimized with residual atomic forces less than 0.01 eV/Å. The resulting electronic structure of the optimized strip is almost the same as that of the unrelaxed graphitic strip, which is consistent with a previous calculation using the model, including the electron-lattice coupling.[22] We also check the dependence of the interlayer distance, but it does not change the energetics between configurations. Thus we use a fixed geometry with the C-C bond length of 1.42 Å, and the interlayer distance of 3.34 Å for the stacked geometry for different electronic and magnetic configurations. For the dihydrogen passivation case, we also carried out full geometry optimizations, but did not find any sizable change in the electronic structure related to the bearded edge structure. For the Brillouin zone (BZ) integration, 15 k points are uniformly selected along the edge direction for the isolated single graphitic strip and 50 k points are sampled over the two-dimensional BZ in the stacked geometry. Since there are a few flat bands as well as dispersive bands near the Fermi level, a large number of k points is required in the BZ integration.

III. MAGNETIC INTERACTIONS IN SINGLE-LAYER STRIPS

A. Total energies for different spin configurations

To investigate the magnetic couplings between the magnetic moments localized at the edges, we examine several spin configurations for the zigzag-edged strip: (i) ferromagnetically ordered spins at both edges with the same spin direction, denoted by FM-F, (ii) ferromagnetically ordered spins at each edge but with the opposite spin directions between the edges, denoted by FM-A, and (iii) antiferromag-

netically ordered spins at each edge, denoted by AF-E. (See Fig. 2 for details.) Note that the FM-F and FM-A configurations have ferromagnetically ordered spins along each edge.

We perform total energy calculations for the strips *without H termination* with the above-mentioned spin configurations and the paramagnetic (PM) state. The total energies, local spin moments, and π state contributions to the edge magnetic moment are listed in Table I. It is found that the ferromagnetic configuration of FM-A is the lowest-energy state with an ordered magnetic moment of $m=1.28$ μ_B per edge-atom. However, the total energy of FM-F is quite close to that of FM-A, with a comparable size of magnetic moments at the edge atoms. The small difference in the total energy between FM-F and FM-A is attributed to the interedge interactions in the strip with a finite width. In Sec. III C, we will show that the two spin configurations, FM-F and FM-A, become degenerate when the two edges are separated by a large strip width W (See Fig. 5).

B. Magnetic coupling mediated by tails of the edge-localized π-orbital states

Contrary to the case of the graphitic strip with H termination,[12] the magnetic moment at the edge without H termination arises from both dangling bonds as well as edge-localized π-orbital states. The dangling bond states localized at the edge contribute significantly to the total magnetic moment with a large exchange splitting of $\sim$2 eV, which in turn enhances the exchange splitting of the π-orbital states localized at the edge. According to the tight-binding analysis[10] on the semi-infinite graphene with a zigzag edge, the π-orbital

TABLE I. The total energies and magnetic moments of an isolated graphitic strip without H termination for various magnetic configurations.

Configuration	Total energy[a] (meV/edge atom)	Magnetic moment (μ_B/edge atom)	π contribution ratio[b] (percentage)
PM	239.9	0.00	
FM-F	2.3	1.19	24.1
FM-A	0.0	1.28	25.3
AF-E	81.4	0.82	12.9

[a]The total energies relative to that of the FM-A configuration with the finite width of $W=8$.
[b]π electron contribution ratio to the edge magnetic moment.

wave functions corresponding to the flat bands are completely localized at the edge sites when $k=\pi$, and exhibit decaying tails into the inner sites as k deviates from π and becomes a fully extended state at $k=2\pi/3$. Due to the lattice symmetry, the tails of the π-orbital wave function, extended into the inner sites of the graphitic strip, reside only at the sites of the sublattice to which the edge atoms belong. Since the edge-localized π-orbital states in a single-layer strip are almost fully spin polarized, the spin-density plot shown in Fig. 2 reveals the spatial distribution of both dangling bond states and the tails of the spin-polarized π-orbital states. In Fig. 2, we label the atomic sites by combining the sublattice and column indices, i.e., $a_1, a_2, b_1, b_2, \ldots$ etc.

To explain why the ferromagnetic edge is favored over the antiferromagnetic one, we compare their total energies and the projected density of states (PDOS). In Figs. 3(a) and 3(b), solid and dotted arrows indicate local magnetic moments and their magnetic tails, respectively. Short solid (dotted) arrows at the a_2 represent the magnetic moments of the magnetic tails stemming from the polarized π-orbital edge states denoted by long solid (dotted) arrows at the $a'_1(a_1)$ site.
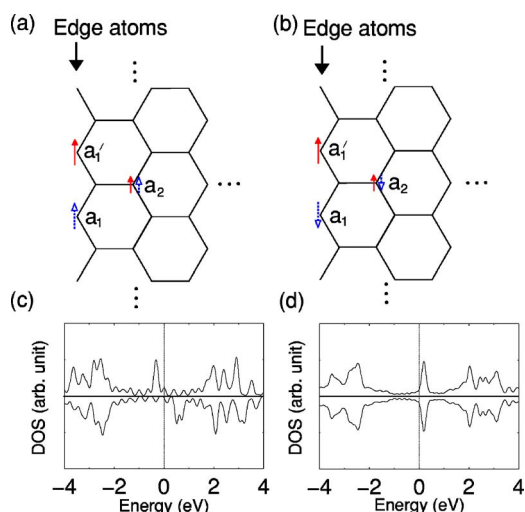

FIG. 3. (Color online) Models of magnetic tails and the corresponding PDOS. (a) and (b) correspond to the ferromagnetic and antiferromagnetic states, respectively. Solid arrows and dotted arrows represent the magnitude and sign of magnetic moments and their tails from different sites. (c) and (d) are the DOS projected at the site a_2 of the (a) ferromagnetic and (b) antiferromagnetic states, respectively.

We find that the ferromagnetic state in Fig. 3(a) contributes constructively to the spin at the site a_2, while the antiferromagnetic states in Fig. 3(b) contribute destructively to the spin at the site a_2. To clarify this point, the density of state (DOS) projected at the site a_2 in Figs. 3(a) and 3(b) is shown in Figs. 3(c) and 3(d), respectively. In the case of AF-E shown by Figs. 3(b) and 3(d), and Table I, the contribution of the π-orbital states diminishes due to the destructive interference between the spin-up and spin-down tails of the edge-localized π-orbital states. Since the net spin polarization of the π orbital is zero in the case of AF-E, there is no exchange splitting of the localized π-orbital states at the Fermi level. On the other hand, the ferromagnetic case shows an enhanced exchange splitting between spin-up and spin-down π-orbital states, as shown in Fig. 3(c), which explains that the total energies of FM-F and FM-A are lower than that of AF-E.

C. The interedge magnetic coupling and its width dependence

The energy difference between the FM-A and FM-F configurations can also be explained by the interference effect between the magnetic tails derived from both edges. As shown in Table I, it is noted that FM-A is the most stable configuration, which is also consistent with previous calculations by Okada and Oshiyama.[12]

The exchange energy gain of FM-A by spin polarization is expected to be larger than that of FM-F because the edge spin configurations of FM-F lead to a destructive interference between the magnetic tails inside the strip. For the clarity, the $W=3$ graphitic strip is shown in Fig. 4. Solid arrows and dotted arrows represent the magnitude and sign of the magnetic moment at each site arising from the magnetic tails of the localized states at the different edge. This model clearly demonstrates that the destructive interference dominates at the inner sites of the strip for FM-F ordering, while the magnetic moments at the inner sites are enhanced for the FM-A configuration. Thus, FM-A becomes energetically more stable than FM-F due to the larger gain of the exchange energy.

Since the magnetic tails have a finite decay length, however, the energy difference between FM-A and FM-F decreases and eventually vanishes as the width of graphitic strip increases beyond the decay length of the tails. Figure 5 demonstrates the width dependence of the energy difference between FM-A and FM-F. The energy difference ΔE_{F-A} be-
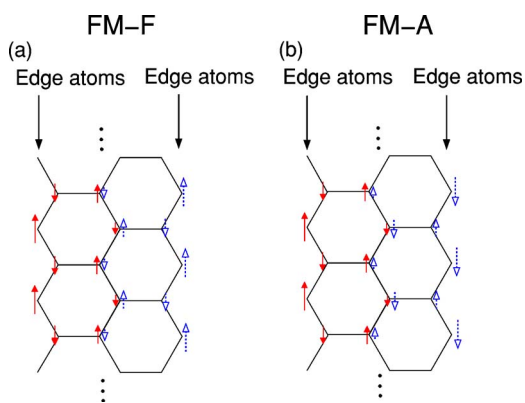
FIG. 4. (Color online) The magnetic tails and the interedge interactions for (a) FM-F and (b) FM-A in the narrow strip of $W=3$. Note that it has opposite spins at the sites belonging to different sublattices. Solid and dotted arrows represent the magnitude and sign of magnetic moments and tails, respectively.

FIG. 6. (Color online) Schematic magnetic moment map of the AB stacking ferromagnetic layer and antiferromagnetically coupled ferromagnetic layers. Filled arrows represent magnetic moments of the A layer and open arrows the magnetic moment of the B layer. The length of the arrows is proportional to the local magnetic moment. The dashed and dash-dotted lines are guides to the eye for understanding the stacking sequences.

tween FM-F and FM-A is always positive, indicating that FM-A is more stable than FM-F, whereas ΔE_{F-A} is reduced as the width of the strip increases, implying that the exchange energy difference accounts for the energy dependence of ΔE_{F-A} on the value of W. As the magnetic moment of the edge without H termination is larger than that with the H passivation, ΔE_{F-A} is larger for the H termination case.

IV. INTERLAYER MAGNETIC COUPLINGS

Now we investigate the effect of stacking on the magnetic structure of the graphitic fragments. Let us consider two different stacking sequences, i.e., AA and AB. The interlayer distance is fixed to that of graphite, 3.34 Å. In the AA stacking, all the atoms in the upper layers are directly above the atoms in the lower layers and vice versa, whereas in the AB stacking, the B layers are shifted by the length of the C-C bond along the bond direction and only a half of the atoms in the upper layers are above the atoms in the lower layers. This means that all the atoms in the AA stacking interact directly with other layers, but in the AB stacking only a half of the atoms do. In Fig. 6, we show a schematic drawing of the geometry and magnetic configurations of the AB-stacked graphitic fragments.
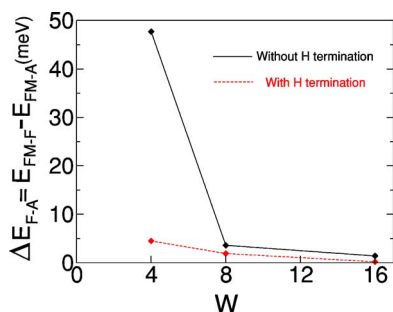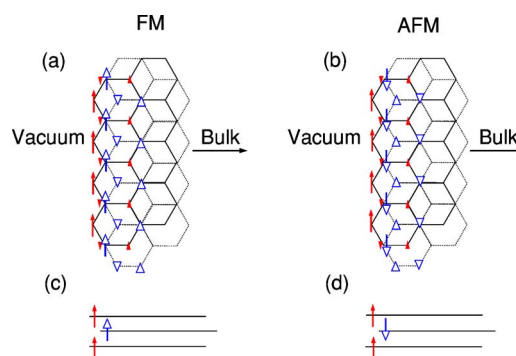

FIG. 5. (Color online) Total energies of FM-F and FM-A depending on the strip width (W). Solid and dashed lines indicate the strips with and without dangling bonds, respectively.

Among the various possible spin configurations, we consider only cases where the local moments within each layer are ferromagnetically ordered. The parallel spin configuration between the edges of the neighboring layers is denoted by FM, and the antiparallel spin configuration between the neighboring layers, by AFM. The total energies, local magnetic moments, and π state contribution to the edge magnetic moment are shown in Table II. Since all π electrons interact directly within the layers in AA stacking cases, it is shown that π-electron contribution to the edge magnetic moment is reduced more than that of AB stacking cases. It can be seen that AB-FM is energetically most stable among the spin configurations considered here. It is also noticeable that AF is favored in the case of the AA stacking, while FM has a lower energy in the case of the AB stacking. To understand the energy difference between the different stacking sequences, we focus on the interlayer coupling of the spin-polarized π-orbital states, which depends on the edge-state polarization.[23] Since the adjacent layers of the AB stacking are shifted by one C-C bond length, the interlayer coupling is mostly conveyed by the interaction between the atoms in the different sublattices of adjacent layers. In Fig. 6, filled and open arrows represent the magnetic moments of the A and B layers, respectively. We note that FM [top view (a), side view (c)] results in the antiferromagnetic coupling between the two nearest carbon atoms in the adjacent layers. Similarly, AFM configuration [top view (b), side view (d)] results in the ferromagnetic interlayer coupling.

Figure 7 shows the DOS for the FM and AFM states in the AA or AB stacking configurations. The localized π-orbital and dangling bond states appear near the Fermi level. The exchange splitting of the dangling bond state, measured by the energy difference between peaks in spin-up and spin-down DOS, is larger than that of the edge-localized π-orbital states. The interlayer interaction is mostly attributed to the π state due to their shape, which is extended along the z direction, while the dangling bond states do not participate in the interlayer interactions. When the edges are passivated by hydrogen atoms, on the other hand, our previous work has shown that the magnetic moment by the local-

TABLE II. Total energy and magnetic moment of the stacked graphitic strips with open edge.

Configuration	Total energy[a] (meV/edge atom)	Magnetic moment (μ_B/edge atom)	π contribution ratio[b] (percentage)
AB-FM	0	1.26	25.1
AB-AFM	2.0	1.26	27.9
AA-FM	72.5	1.03	16.0
AA-AFM	40.5	1.00	16.0

[a]Energy difference relative to that of the AB-FM configuration.
[b]π electron contribution ratio to edge magnetic moment.

ized π-orbital states disappear upon the stacking.[13] It was also concluded that the magnetic polarization of π states localized at the edge is enhanced by the magnetic moment of the dangling bond state.

V. EDGE-LOCALIZED π-ORBITAL STATES IN A STRIP WITH DIHYDROGENATED ZIGZAG EDGES

While the localized flat band in the range of $2\pi/3 \leqslant |k| \leqslant \pi$ in the BZ is considered the origin of magnetism in graphitic fragments, a bearded edge state,[16,24] as well as the magnetic proximity effect of a magnetic impurity such as Fe atoms, were also suggested as possible origins. Here we try to probe more detailed features of the edge states. In the bearded edge, each carbon atom at the zigzag edge is connected with two hydrogen atoms so that the edge carbon atom becomes tetrahedrally coordinated. To reduce the small width effect, we calculate the band structure of a similar but longer geometry ($W=8$) than those in previous calculations,[16] as illustrated in Fig. 8. When the width of strip is smaller, two different edge states in different edge can be misconceived as a intrinsic property of nanographite.

Two different configurations are considered: (i) ferromagnetically ordered spins at both edges denoted by FM and (ii) antiferromagnetically ordered spin at both edges denoted by AFM. Figures 8(a) and 8(b) show the band structure of the majority and minority spins of the FM configuration. Figures 8(c) and 8(d) are the band structure of the up- and down-spins of the AFM configuration. It is found that the FM configuration has a lower energy than the AFM configuration by 4.9 meV per edge atom. As is shown in Figs. 8(e) and 8(f), the fact that two states at the Γ and X points near the Fermi level are in the same sublattice looks consistent with our tail interaction picture. That is, the FM configuration should have a lower energy than the AF configuration due to the magnetic tails' interaction, maximizing the exchange energy gain. While the band structure of the FM configuration is consistent with previous work,[16] we present the band structures of both FM and AFM configurations to clarify the character of bearded-edge states. In Fig. 8, the state at the Γ point(open triangle) is the bearded-edge state and the state at the X point (solid triangle) is the edge-localized π-orbital state. The large change of the band dispersion near the $k=2\pi/3$ point implies that the characters of the states at the Γ and X points are different, which is confirmed by the charge density plots of the states shown in Figs. 8(e) and 8(f). By introducing an additional hydrogen atom to each H-terminated edge, the remaining π electron changes into the σ-bonding state. Thus, the outermost edge atoms have no π-orbital state contributing to the states near the Fermi level.

To investigate the band structure of monohydrogenated and dihydrogenated graphite strips, we perform tight-binding calculations with a large width ($W=3000$), which is completely free of the interedge interaction. When both edges are monohydrogenated, as shown in Fig. 9(a), one can identify localized π-orbital edge states at $2\pi/3 \leqslant |k| \leqslant \pi$, as shown in Fig. 9(e). The strip with dihydrogenated edges in Fig. 9(b) has localized edge states at $0 \leqslant |k| \leqslant 2\pi/3$, as shown in Fig. 9(h). With both types of edges present, the flat band in the whole range of band structure is shown in Figs. 9(c) and 9(f). Obviously, the flat bands in $0 \leqslant |k| \leqslant 2\pi/3$ come from the localized states at the dihydrogenated edge, while those in $2\pi/3 \leqslant |k| \leqslant \pi$ come from those in the monohydrogenated edge.

To understand the band structure of the bearded edge, we consider the one-orbital tight-binding approach. The eigenstates can be expanded with a tight-binding basis as follows
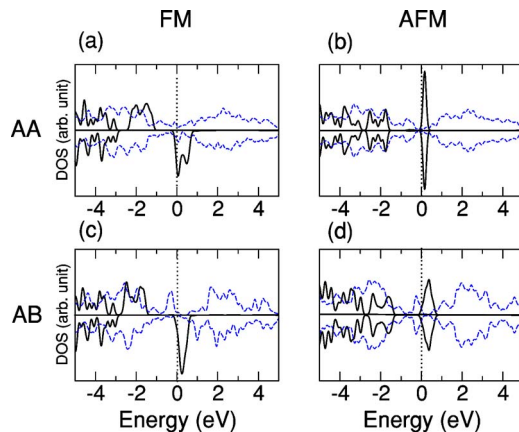

FIG. 7. (Color online) The DOS of the graphite fragment with AA stacking and AB stacking. AA-stacked FM, AA-stacked AFM, AB-stacked FM, and AB-stacked AFM are shown in (a), (b), (c), and (d) respectively. Solid (black) and dotted lines are DOS of the σ states and π states, respectively. See Fig. 6 for the detailed spin configurations.

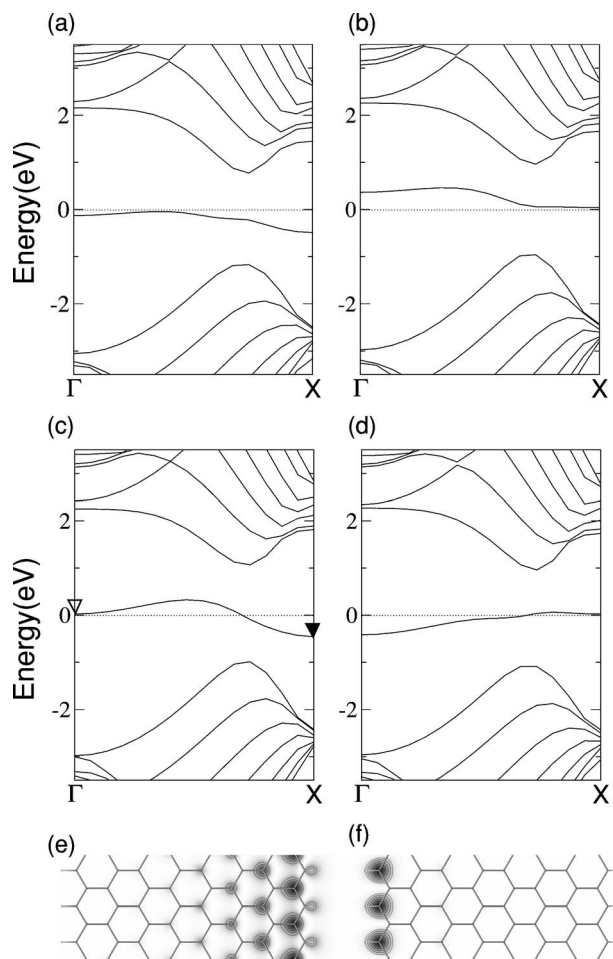$$\psi_{n,k} = \frac{1}{\sqrt{N}} \sum_{l=1} C_{n,k}^l \phi_n^l. \qquad (1)$$

FIG. 8. The band structure of the graphitic strip with monohydrogenation on the left side and dihydrogenation on the right side of the graphene sheet. See the Fig. 9(c) for the geometry. (a) and (b) are the band structure of the majority and minority spins of the FM configuration. (c) and (d) are the band structure of the up- and down-spins of the AF configuration. (e) and (f) are the contour plots of the charge density of the states at the Γ point (marked by an open triangle) and the X point (marked by a solid triangle) of the up-spin of (c), respectively.

Here N is a normalization constant, $C_{n,k}^{l}$ is a coefficient, and ϕ_{n}^{l} is a p_z orbital tight-binding wave function at the site l, where the atomic index in a sublattice starts from the edge site. By applying the boundary condition corresponding to the dihydrogenated edge as discussed above and the zigzag boundary condition for each case, the solution for each sublattice at $E=0$ are given by

$$|C_{n,k}^{l}| = \left[\sqrt{\frac{1}{2[1+\cos(ka)]}} \right]^{(l-1)} |C_{n,k}^{1}|, \quad \left(0 \leqslant ka \leqslant \frac{2\pi}{3}\right),$$

(2)

$$|C_{n,k}^{l}| = \left[\sqrt{2\cos\left(\frac{ka}{2}\right)} \right]^{(l-1)} |C_{n,k}^{1}|, \quad \left(\frac{2\pi}{3} \leqslant ka \leqslant \pi\right),$$

(3)

where a is a one-dimensional lattice constant. The square brackets can be regarded as the decaying factors, which are
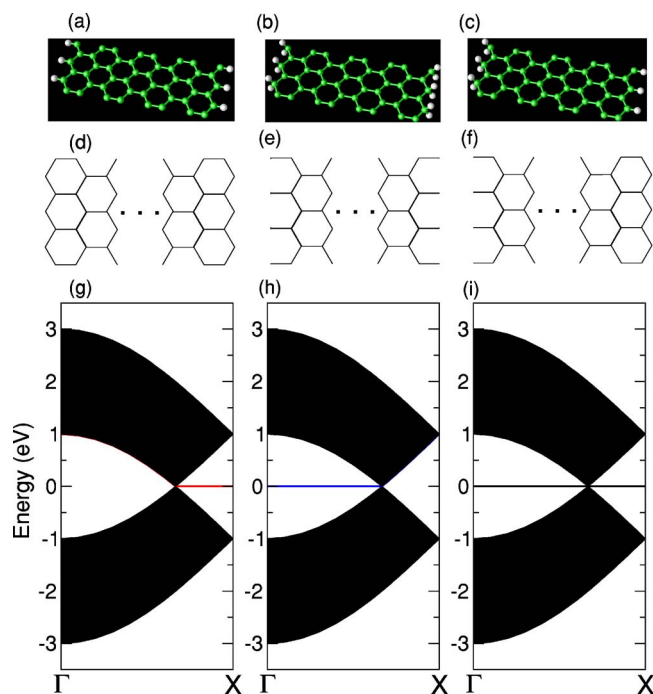

FIG. 9. (Color online) Geometric structures for the strip with (a) monohydrogenation in both edges, (b) dihydrogenation in both edges, (c) monohydrogenation in one edge and dihydrogenation in the other edge. (d), (e), and (f) are schematic drawings of the strip with a large width for the edge configurations (a), (b), and (c), respectively. (g), (h), and (i) are one-orbital tight-binding band structures for the large width strip ($W=3000$) with edge configurations corresponding to (a), (b), and (c), respectively. Note that the models shown in (a), (b), and (c) is the strip with $W=8$.

the geometrical progression factors between the amplitude of wave functions in the same sublattice. When the decaying factor is less than 1, the state becomes an edge state. When it equals 1 however, the state becomes a bulk state. The decaying factor of the bearded state runs from 0.5 to 1 as k increases from 0 to $2\pi/3$. Since the decaying factor of the most localized bearded state is 0.5, the bearded states are less localized than the localized edge state with π state, which can have a decaying factor equal to 0, as shown in Fig. 8.

From the first-principles calculations on the bearded edge, we find that the exchange splitting of a bearded-edge state is ~ 0.5 eV, which is similar to the value of the π-orbital edge state. This is consistent with previous work.[16] Thus, the exchange interaction of the bearded state may not be strong enough to trigger the formation of macroscopic magnetic moments when the layers are stacked.[13]

VI. DISCUSSION

The magnetic proximity effect in the presence of a magnetic impurity is considered by a model consisting of a graphene sheet and an iron atom attached at the zigzag edge. Another possible model is the graphitic strips where iron atoms are intercalated at the zigzag edge. (See Fig. 10.) When we investigate these model structures with the first-principles methods, no magnetism is found to be associated
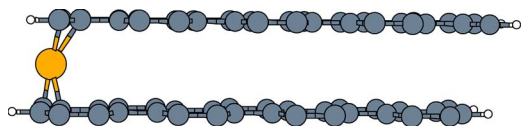
FIG. 10. (Color online) Model geometry of iron-intercalated graphite. Dark and light gray color denote an iron and carbon atoms, respectively. The small white circles represent the position of the hydrogen atoms.

with the carbon atoms. In contrast to the case of the dangling bond states, the localized π-states shift slightly above the Fermi level and do not contribute to the local magnetic moment. From these results, we understand that the dangling bond states are crucial to the understanding of magnetism in graphitic fragments. As our previous work[13] indicates, the graphitic fragments without dangling bond states, i.e., the H-passivated model, turns out to be nonmagnetic when they are stacked. This can be expected from the small exchange splitting of the localized edge state (~ 0.5 eV) in the single-layer graphene sheet. On the other hand, the exchange splitting of the dangling bond state is ~ 2.3 eV, large enough to induce magnetic instability and to enhance the exchange splitting of the localized π-orbital state up to ~ 1.2 eV. Although it was suggested that the magnetic proximity effect can occur due to the Fe_3O_4 magnetic impurity,[7] which has been considered as a half-metallic ferromagnet in the bulk form, the role of iron oxide on the magnetism in carbon systems is not yet clear.

Although the origin of magnetism in carbon systems is still controvesial, we suggest the stacked graphitic fragments as a source of the observed magnetic behavior. As shown in Fig. 5, the interedge interaction diminishes as the width of the strip increases so that both the FM and AFM interedge orderings become almost degenerate. Thus, when the size of the stacked graphitic fragments become larger than 5 nm, the FM-ordered moments at each edge, i.e., stacked edge surface become enhanced by the interlayer interactions and result in a macroscopic magnetic ordering. Assuming a favorable situation in a realistic sample, let us try to estimate the condition of the dangling-bond states to the observed magnetism. For the graphitic fragment of the width larger than ~ 5 nm, about $1/12$ of the total number of the carbon atoms in the fragments are estimated to belong to the edge surface and to contribute to the FM moment. This would lead to the magnetic signal ranging up to ~ 1 em/g, with the stacked graphitic fragment. In experiments, the characteristic magnitude of the magnetic signal is $\sim 10^{-3}$ emu/g for glassy carbon[8] and is 10^{-6} emu/g for proton-irradiated graphite.[9] Thus, if

the ratio of this unsaturated nanographite fragment could be in the range of $0.1\% \sim 0.0001\%$, depending on the sample configuration, it is reasonable to consider it as a possible origin of the observed magnetism.

VII. SUMMARY

While experiments on the magnetism of organic materials, in particular graphitic ones, can be interpreted as indirect or direct evidence of carbon magnetism, a solid theoretical framework is still under development to give a good description of these observations. Although it is clear that the mechanism for the long-range ordering, rather than the magnitude of local moment, is crucial for explaining the magnetism of a graphitic fragment, it has not been discussed much so far. Based on this work, a plausible theoretical calculation was done for an explanation of the experiments. We studied the vacancy-induced magnetic structure in a graphene sheet. The details and discussion will be published elsewhere.

Focusing on the ordering between the local moments, we performed first-principle calculations on the nanosize graphitic fragments. The magnetism of the graphitic edge is well understood by considering the magnetic tails' interaction and the antiferromagnetic interlayer coupling. The ferromagnetic ordering at only one side is found to enhance the magnetic energy gain. As for the interedge interactions, the antiferromagnetic coupling between the edge states is favored, but the energy lowering relative to the ferromagnetic coupling decreases as the strip width increases.

The origin and characters of dihydrogenated edge states are identified by first-principle calculations as well as the tight-binding method. It is found that the additional hydrogen passivation attached on the zigzag edge can induce a change of the boundary condition and another type of edge state appears. The dihydrogenated edge state may contribute to the carbon magnetism, but it is likely to disappear when stacked. The magnetic proximity effect due to a magnetic impurity such as Fe atoms is also found to be negligible. Overall, we suggest that the presence of a dangling band is most crucial to the formation of the carbon magnetism. The localized edge states or magnetic impurity may not be significant in the stacked graphitic systems.

ACKNOWLEDGMENTS

*Corresponding author. Email: jyu@snu.ac.kr

[1] A. Mrzel, A. Omerzu, P. Umek, D. Behalves, Z. Juliečić, and Z. Trontelj, Chem. Phys. Lett. **298**, 329 (1998).

[2] P. Esquinazi, A. Setzer, R. Höhne, C. Semmelhack, Y. Kopelevich, D. Spemann, T. Butz, B. Kohlstrunk, and M. Lösche, Phys. Rev. B **66**, 024429 (2002).

[3] P. O. Lehtinen, A. S. Foster, A. Ayuela, A. Krasheninnikov, K. Nordlund, and R. M. Nieminen, Phys. Rev. Lett. **91**, 017202 (2003).

[4] Y. Shibayama, H. Sato, T. Enoki, and M. Endo, Phys. Rev. Lett.

84, 1744 (2000).

[5] A. Omerzu, D. Mihailovic, and M. Tokumoto, Phys. Rev. B **61**, R11883 (2000).

[6] T. L. Makarova, B. Sundqvist, R. Höhne, P. Esquinazi, Y. Kopelevich, P. Scharff, V. A. Davydov, L. S. Kashevarova, and A. V. Rakhmanina, Nature **413**, 716 (2001).

[7] J. M. D. Coey, M. Venkatesan, C. B. Fitzgerald, A. P. Douvalis, and I. S. Sanders, Nature **420**, 156 (2002).

[8] X. Wang, Z. X. Liu, Y. L. Zhang, F. Y. Li, R. C. Yu, and C. Q. Jin, J. Phys.: Condens. Matter **14**, 10265 (2002).

[9] P. Esquinazi, D. Spemann, R. Höhne, A. Setzer, K.-H. Han, and T. Butz, Phys. Rev. Lett. **91**, 227201 (2003).

[10] M. Fujita, K. Wakabayashi, K. Nakada, and K. Kusakabe, J. Phys. Soc. Jpn. **65**, 1920 (1996).

[11] Y. Miyamoto, K. Nakada, and M. Fujita, Phys. Rev. B **59**, 9858 (1999).

[12] S. Okada and A. Oshiyama, Phys. Rev. Lett. **87**, 146803 (2001).

[13] H. Lee, N. J. Park, Y.-W. Son, S. Han, and J. Yu, Chem. Phys. Lett. **398**, 207 (2004).

[14] N. Park, M. Yoon, S. Berber, J. Ihm, E. Osawa, and D. Tománek, Phys. Rev. Lett. **91**, 237204 (2003).

[15] P. O. Lehtinen, A. S. Foster, Y. Ma, A. V. Krasheninnikov, and R. M. Nieminen1, Phys. Rev. Lett. **93**, 187202 (2004).

[16] K. Kusakabe and M. Maruyama, Phys. Rev. B **67**, 092406 (2003).

[17] P. Hohenberg and W. Kohn, Phys. Rev. **136**, B864 (1964).

[18] W. Kohn and L. J. Sham, Phys. Rev. **140**, A1133 (1965)

[19] See S. Baroni, A. Dal Corso, S. de Gironcoli, and P. Giannozzi, http://www.pwscf.org.

[20] D. Vanderbilt, Phys. Rev. B **41**, R7892 (1990).

[21] J. P. Perdew and Y. Wang, Phys. Rev. B **33**, R8800 (1986); **45**, 13244 (1992).

[22] M. Fujita, M. Igami, and K. Nakada, J. Phys. Soc. Jpn. **66**, 1864 (1997).

[23] The present results are based on the LSDA calculations. It is noted that there remain subtleties in regard to the use of LSDA for the energetics study of the carbon systems with the van der Waals interatomic distance, which requires further investigations.

[24] D. J. Klein, Chem. Phys. Lett. **217**, 261 (1994)